International Journal of Minerals, Metallurgy and Materials
Volume 21, Number 6, June 2014, Page 577
DOI: 10.1007/s12613-014-0944-3

Microstructure and mechanical properties of the welding joint filled with microalloying 5183 aluminum welding wires

Zhen Xu, Zhi-hao Zhao, Gao-song Wang, Chao Zhang, and Jian-zhong Cui

The Key Laboratory of the Ministry of Education of China for Electromagnetic Processing of Materials, Northeastern University, Shenyang 110819, China
(Received: 25 November 2013; revised: 7 January 2014; accepted: 18 January 2014)

Abstract: In this study, 7A52 aluminum alloy sheets of 4 mm in thickness were welded by tungsten inert gas welding using microalloying welding wires containing traces of Zr and Er. The influence of rare earth elements Zr and Er on the microstructure and mechanical properties of the welded joints was analyzed by optical microscopy, energy dispersive X-ray spectroscopy, transmission electron microscopy, hardness testing, and tensile mechanical properties testing. Systematic analyses indicate that the addition of trace amounts of Er and Zr leads to the formation of fine Al_3Er, Al_3Zr, and $Al_3(Zr,Er)$ phases that favor significant grain refinement in the weld zone. Besides, the tensile strength and hardness of the welded joints were obviously improved with the addition of Er and Zr, as evidenced by the increase in tensile strength and elongation by 40 MPa and 1.4%, respectively, and by the welding coefficient of 73%.

Keywords: aluminum alloys; inert gas welding; rare earth elements; microalloying; joints; microstructure; mechanical properties

1. Introduction

Al–Zn–Mg series alloys have been widely utilized in aerospace and automotive industries owing to their exceptional characteristics including high strength, good fracture toughness, low density, and low cycle fatigue [1–3]. The microstructure of the alloy often plays an important role in determining their mechanical properties. Conventional tungsten inert gas (TIG) welding results in microstructure coarsening and a decrease in the mechanical properties of welded joints, obviously due to high heat applied during the welding process [4–5]. Previous studies [6–7] have indicated that the mechanical properties of the welded joint are mainly determined by welding wires.

In principle, the addition of some trace elements to the aluminum alloy can refine the microstructure and consequently enhance the strength of the alloys. To this end, some studies [8–21] have reported the effect of Sc on the microstructural and mechanical properties of aluminum alloys. According to these studies, the addition of Sc can significantly improve the mechanical properties due to the formation of elastically hard and coherent Al_3Sc particles with $L1_2$ crystal structure, which can strongly refine grains and inhibit re-crystallization. However, the commercial feasibility of this approach is greatly limited by the high cost of Sc. According to the study reported by Nie, Wen, Wu, *et al.* [22–25], addition of a small amount of Er, which is cheaper than Sc, has similar effects on the microstructure and mechanical properties of aluminum alloys.

Therefore, in the present study, 7A52 aluminum alloy sheets of 4 mm in thickness have been welded by TIG welding using microalloying welding wires containing traces of Zr and Er. Based on systematic analyses, we have studied the influence of Zr and Er on the microstructure and mechanical properties of the welded joint.

2. Experimental

In this study, the 7A52 aluminum alloy sheet of 4 mm in thickness was subjected to a solution treatment at 470°C for 1 h [26], followed by water quenching and subsequent aging at 105°C for 8 h and at 130°C for 14 h. The aluminum welding wires used in this study were prepared by extrusion and drawing processes. The chemical compositions of the 7A52 aluminum alloy base metal and 5183 aluminum alloy

Corresponding author: Zhi-hao Zhao E-mail: zzh@epm.neu.edu.cn

welding wires are summarized in Table 1. Prior to the welding process, the surfaces of the base metal and welding wires were cleaned with organic solvent. Subsequently, TIG welding was performed in the direction perpendicular to the rolling direction of the base metal. The experimental parameters adopted during the welding process are summarized in Table 2.

Table 1. Chemical composition of the base metal and welding wires used in this study wt%

Sample	Mg	Mn	Ti	Cu	Cr	Zn	Zr	Er	Al
Base metal	2.1	0.30	0.08	0.08	0.16	4.2	0.14	—	Bal.
Wire a	4.7	0.80	0.10	—	—	—	—	—	Bal.
Wire b	4.7	0.80	0.10	—	—	—	0.10	0.4	Bal.

Table 2. TIG welding parameters

Welding current, I / A	Welding voltage, U / V	Welding speed, v / (mm·s^{-1})	Shielding gas	Gas flux, Q / (L·min^{-1})
120–180	18–20	0.8	Ar	15

The microstructure of welded joints was observed by optical microscopy (OM, DMI5000M) and transmission electron microscopy (TEM). Specimens for optical observation were taken along the rolling direction and etched using the Keller's reagent. Similarly, specimens for TEM observation were cut from the weld zone of the welded joints, mechanically machined, ground, and prepared as 3 mm discs of 80 μm in thickness. The obtained discs were punched and electropolished by the double-jet technique in an electro-polishing solution containing the mixture of 30vol% HNO_3 and 70vol% CH_3OH at −25°C and 15 V. The tensile strength of the welded joints (4 mm × 25 mm × 100 mm) was evaluated using an SANS CMT-5105 universal test machine at the tensile velocity of 2 mm/min at room temperature. The surface of the welded joint was milled prior to tensile testing. The value reported in this study is the average value of three tensile tests. The typical fractured surfaces of welded joints were observed by scanning electron microscopy (SEM). The Vickers hardness of specimens was measured on the transverse cross-section of the welded joints, along the half thickness line, using the 452-SVD vickers hardness tester at the load of 49 N.

3. Results

3.1. Mechanical properties

Fig. 1 shows the hardness distribution on the cross-section of welded joints. As is seen, the hardness distribution trend is almost the same for both the welded joints, with symmetrical distribution on either side of the center of the welded joints as the axis. In the entire welded joint, the weld zone and the heat-affected zone are found to be the weakest areas, with the lowest hardness of the welded joints appearing at the center of the weld zone. The hardness values of welding wires a and b are Hv 78 and Hv 88, respectively. As the trend traverses outwards from the center to the base metal, there appears a hardness peak in the fusion zone, about 4 mm away from the center. With the drop of hardness in the heat-affected zone, it significantly increases to Hv 135 in the base metal, about 8 mm away from the center. Comparing the hardness distribution curves shown in Fig. 1, it can be observed that the hardness of the welding joint with the microalloying aluminum welding wire is higher than that with the traditional 5183 aluminum welding wire, especially at the welding zone.

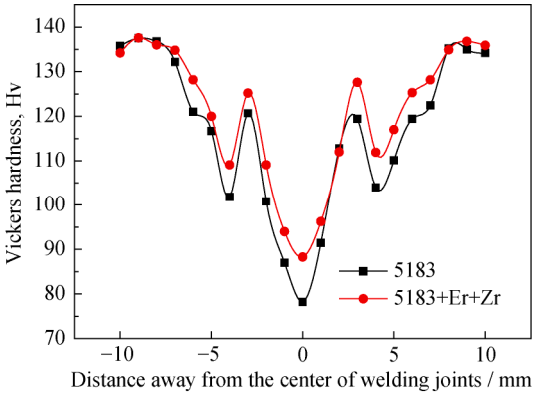

Fig. 1. Vickers hardness distribution of welded joints.

Table 3 presents the tensile properties of the base metal and welded joints obtained with two kinds of welding wires (microalloying aluminum welding wire and traditional 5183 aluminum welding wire). It can be seen that the tensile strength, yield strength, and elongation of the base metal are superior to those of welded joints. Compared to the welded joint filled with the traditional 5183 aluminum welding wire, the tensile strength and yield strength of the welded joint with the microalloying welding wire increased by 40 and 10 MPa, respectively. Besides, the elongation was about 1.4% higher. More importantly, the welding coefficient was improved from 64.2% to 73.0% by the use of the microalloying welding wire.

The tensile testing results suggest that all the fractures occur at the weld zone, consistent with the hardness testing results. SEM images of the typical fractured surfaces of welded joints are shown in Fig. 2. As is seen, the fractured surfaces of both the welded joints predominantly consist of dimples. Nevertheless, we could observe some obvious disparities between them. In the case of the welded joint with

the microalloying welding wire, the fractured surface showed uniform distribution of smaller dimples containing several secondary phases.

3.2. Microstructure

In general, welded joints consist of the weld zone (WZ), fusion zone (FZ), and heat-affected zone (HAZ). Fig. 3 shows the microstructure of welded joints with the traditional 5183 welding wire and microalloying welding wire. As evidenced from the figure, both the weld zones exhibit an equiaxial crystal structure, while grain size in Figs. 3(c) and 3(d) is much finer than that in Figs. 3(a) and 3(b). In addition, the fusion zones of both the welded joints are not characterized by any visible columnar crystals. On the other

Table 3. Mechanical properties of the base metal and welding joints

Sample	Tensile strength / MPa	Yield strength / MPa	Elongation / %	Welding coefficient	Cracked position
Base metal	452.2	374.1	12.5	—	—
Welding joint a	290.3	200.3	8.0	64.2 %	Weld zone
Welding joint b	330.2	210.3	9.4	73.0 %	Weld zone

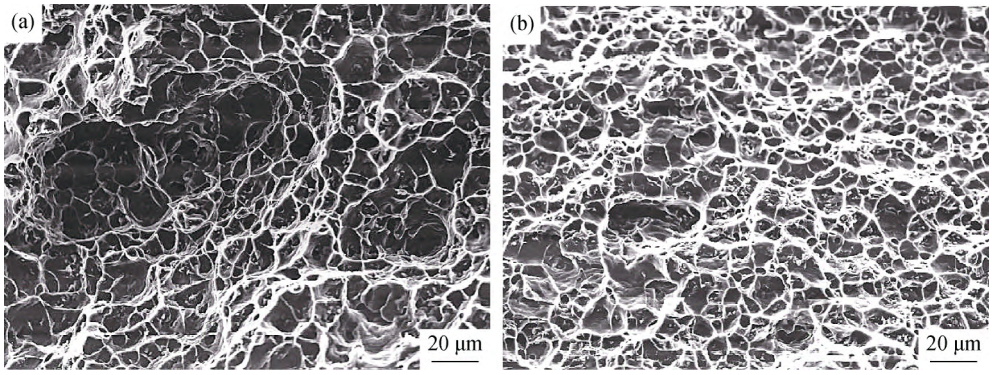

Fig. 2. SEM images showing the typical fractured surfaces of welded joints: (a) with the traditional 5183 wire; (b) with the microalloying 5183 wire.

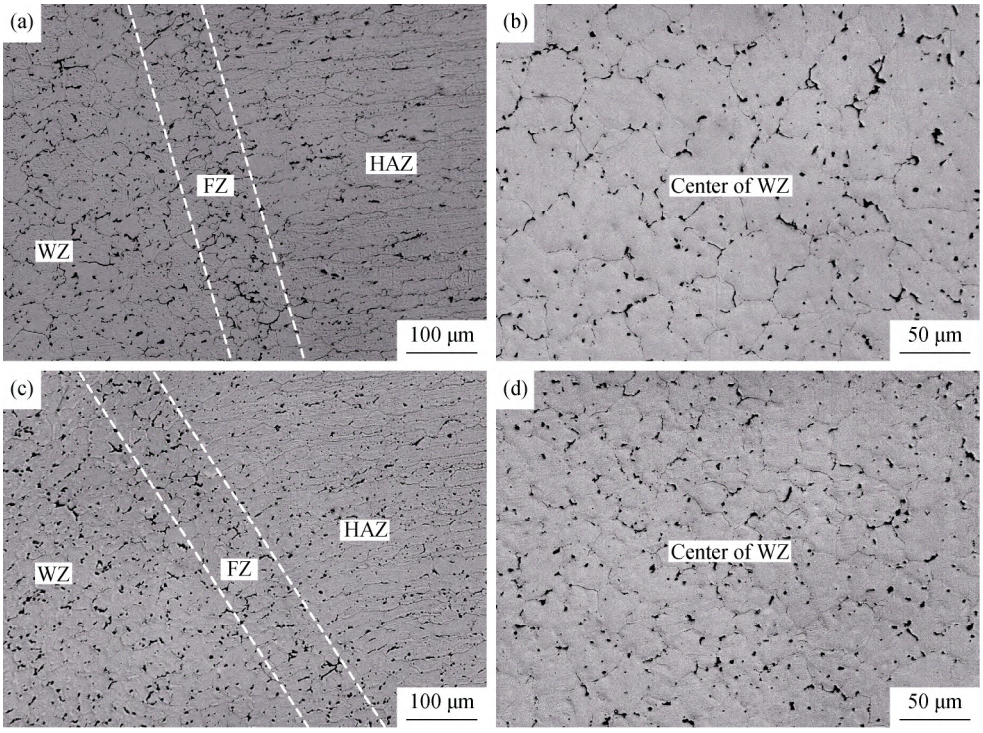

Fig. 3. Optical images of welded joints with two kinds of welding wires: (a, b) with the traditional 5183 wire; (c, d) with the microalloying 5183 wire.

hand, the wide range of the heat-affected zone in both the welded joints is mainly composed of fibrous tissues. However, the grains in the welded joint obtained using the traditional welding wire were relatively coarser than those obtained with the microalloying welding wire.

3.3. TEM observation

Fig. 4 shows the TEM images of the welded joint obtained with the microalloying welding wire. The images indicate the formation of a large amount of nanoparticles, which are considered as Al_3Er and $Al_3(Zr,Er)$, around grain boundaries. During the welding process, Zr and Er in the welding wire dissolved into the welding zone and formed a supersaturated solid solution, upon cooling at a rapid cooling rate. With subsequent natural aging, Zr and Er appeared in the welded joint as nano-sized particles.

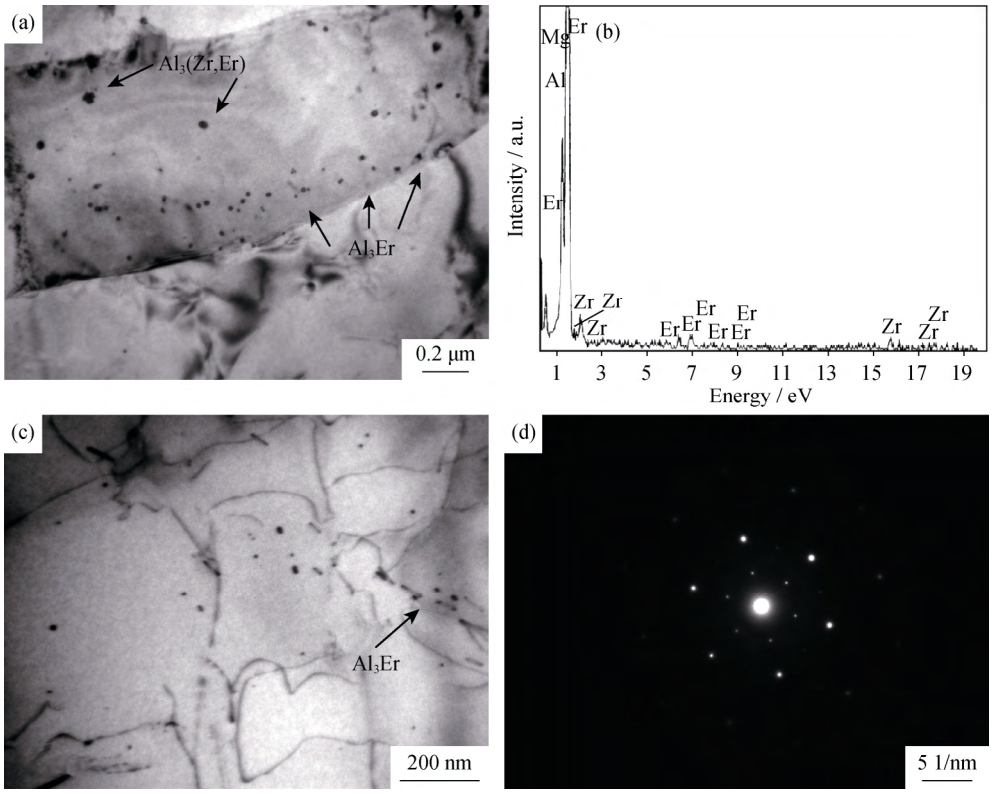

Fig. 4. TEM images of the welded joint with the microalloying welding wire containing Zr and Er: (a, c) typical $Al_3(Zr,Er)$ and Al_3Er particles; (b) energy dispersive X-ray spectrum; (d) selected area diffraction pattern.

4. Discussion

4.1. Grain refinement

As can be seen from Fig. 2, grains in the weld zone of the welded joint with the microalloying welding wire are much finer and more uniform than those obtained with the traditional 5183 welding wire. This could be attributed to Zr and Er contents in the welding wire. In this case, during the solidification of the weld zone, Zr and Er in the welding wire enriched at the front of the advancing solid-liquid interface. This resulted in the formation of primary Al_3Zr, Al_3Er, and $Al_3(Zr,Er)$ phases in the melt, when the content approached the eutectic point. Subsequently, they were pushed to the grain boundary. These phases with $L1_2$ crystal structure could lead to obvious grain refinement due to low lattice parameter mismatches between the phases and the Al matrix. Besides, these nano-scale phases acted as heterogeneous nuclei, thereby increasing the nucleation rate and facilitating grain refinement in the weld zone. Moreover, these primary particles are considered to prevent grain growth, which is also beneficial for grain refinement.

4.2. Improvement of mechanical properties

As can be seen from Table 3 and Fig. 1, the use of the microalloying welding wire containing Zr and Er improves the mechanical properties of the welded joint. As mentioned earlier, the microstructure of the welded joint, as determined by the chemical composition of the welding wires filled in the welded joints, leads to the intensification of mechanical properties. The grain refinement in the weld zone and inhibition of re-crystallization in the heat-affected zone observed in the welding process using the microalloying

welding wire result in improved mechanical properties.

According to the Hall-Petch relationship between grain size and strength, the decrease in grain size results in the improvement of tensile strength. Therefore, it is expected that the use of the welding wire containing Zr and Er will contribute to improving the strength of the welding joint.

The corresponding TEM image of the welded joint indicated the formation of nano-sized particles near dislocations within the grain. These particles are considered as secondary precipitations with $L1_2$-type ordered face-centered cubic structure. Rapid cooling in the welding process favored the formation of supersaturated solid solution containing Zr and Er in the Al matrix. Subsequently, during the natural aging process, the fine and dispersed secondary particles precipitated from the supersaturated solid solution and distributed near grain boundaries and dislocations. These secondary particles play an important role in increasing the strength of the welded joints. The movement of dislocations and grain boundaries will be restrained by the particles, thereby demanding more energy for the dislocations and grain boundaries to pass the particles. These results indicate that the use of the microalloying welding wire containing Er and Zr will significantly improve the mechanical properties of welded joints.

5. Conclusions

(1) All the fractures occur at the weld zone, indicating that the weld zone is the weakest area of the whole welding joint. Grain refinement in this area can be realized using the microalloying welding wire containing Zr and Er.

(2) The addition of Er and Zr can improve the mechanical properties of the welded joint due to the effects of fine-grain strengthening and dispersion strengthening. Compared with the use of the traditional 5183 aluminum alloy welding wire, the tensile strength and elongation were increased by 40 MPa and 1.4%, respectively, and the welding coefficient of 73% was achieved using the microalloying welding wire.

References

[1] M. Dixit, R.S. Mishra, and K.K. Sankaran, Structure-property correlations in Al 7050 and Al 7055 high-strength aluminum alloys, *Mater. Sci. Eng. A*, 478(2008), No. 1-2, p. 163.

[2] L.M. Yan, J. Shen, J.P. Li, Z.B. Li, and X.D. Yan, Deformation behavior and microstructure of an Al–Zn–Mg–Cu–Zr alloy during hot deformation, *Int. J. Miner. Metall. Mater.*, 17(2010), No. 1, p. 46.

[3] C. Yang, W.M. Guo, H.X. Zhang, R. Qiu, J. Hou, and Y.B. Fu, Study on the corrosion behavior of 7A52 Al alloy welded joint by electrochemical method, *Int. J. Electrochem. Sci.*, 8(2013), No. 7, p. 9308.

[4] D.X. Yang, X.Y. Li, D.Y. He, H. Hang, and L. Zhang, Study on microstructure and mechanical properties of Al–Mg–Mn–Er alloy joints welded by TIG and laser beam, *Mater. Des.*, 40(2012), p. 117.

[5] Y.S. Sato, P. Arkom, H. Kokawa, T.W. Nelson, and R.J. Steel, Effect of microstructure on properties of friction stir welded Inconel alloy 600, *Mater. Sci. Eng. A*, 477(2008), No. 1-2, p. 250.

[6] A.F. Norman, K. Hyde, F. Costello, S. Thompson, S. Birley, and P.B. Prangnell, Examination of the effect of Sc on 2000 and 7000 series aluminium alloy castings: for improvements in fusion welding, *Mater. Sci. Eng. A*, 354(2003), No. 1-2, p. 188.

[7] S. Dev, A.A. Stuart, R.C.R.D. Kumaar, B.S. Murty, and K.P. Rao, Effect of scandium additions on microstructure and mechanical properties of Al–Zn–Mg alloy welds, *Mater. Sci. Eng. A*, 467(2007), No. 1-2, p. 132.

[8] C. Booth-Morrison, D.C. Dunand, and D.N. Seidman, Coarsening resistance at 400°C of precipitation-strengthened Al–Zr–Sc–Er alloys, *Acta Mater.*, 59(2011), No. 18, p. 7029.

[9] A.K. Mukhopadhyay, A. Kumar, S. Raveendra, and I. Samajdar, Development of grain structure during superplastic deformation of an Al–Zn–Mg–Cu–Zr alloy containing Sc, *Scripta Mater.*, 64(2011), No. 5, p. 386.

[10] M.E. van Dalen, T. Gyger, D.C. Dunand, and D.N. Seidman, Effects of Yb and Zr microalloying additions on the microstructure and mechanical properties of dilute Al–Sc alloys, *Acta Mater.*, 59(2011), No. 20, p. 7615.

[11] K.E. Knipling, D.N. Seidman, and D.C. Dunand, Ambient- and high-temperature mechanical properties of isochronally aged Al–0.06Sc, Al–0.06Zr and Al–0.06Sc–0.06Zr (at.%) alloys, *Acta Mater.*, 59(2011), No. 3, p. 943.

[12] Z.X. Liu, Z.J. Li, M.X. Wang, and Y.G. Weng, Effect of complex alloying of Sc, Zr and Ti on the microstructure and mechanical properties of Al–5Mg alloys, *Mater. Sci. Eng. A*, 483-484(2008), p. 120.

[13] V. Singh, K.S. Prasad, and A.A. Gokhale, Effect of minor Sc additions on structure, age hardening and tensile properties of aluminium alloy AA8090 plate, *Scripta Mater.*, 50(2004), No. 6, p. 903.

[14] I. Halevy, O. Beeri, and J. Hu, Sc-strengthened commercial purity aluminum under high pressure, *J. Mater. Sci.*, 45(2010), No. 3, p. 589.

[15] C.B. Fuller, A.R. Krause, D.C. Dunand, and D.N. Seidman, Microstructure and mechanical properties of a 5754 aluminum alloy modified by Sc and Zr additions, *Mater. Sci. Eng. A*, 338(2002), No. 1-2, p. 8.

[16] Y.A. Filatov, V.I. Yelagin, and V.V. Zakharov, New Al–Mg–Sc alloys, *Mater. Sci. Eng. A*, 280(2000), No. 1, p. 97.

[17] R.R. Sawtell and C.L. Jensen, Mechanical properties and microstructures of Al–Mg–Sc alloys, *Metall. Trans. A*, 21(1990), No. 1, p. 421.

[18] G. Lapasset, Y. Girard, M.H. Campagnac, and D. Boivin, Investigation of the microstructure and properties of a friction stir welded Al–Mg–Sc alloy, *Mater. Sci. Forum*, 426-432(2003), p. 2987.

[19] S. Lee, A. Utsunomiya, H. Akamatsu, K. Neishi, M. Furukawa, Z. Horita, and T.G. Langdon, Influence of scandium and zirconium on grain stability and superplastic ductilities in ultrafine-grained Al–Mg alloys, *Acta Mater.*, 50(2002), No. 3, p. 553.

[20] F. Fazeli, W.J. Poole, and C.W. Sinclair, Modeling the effect of Al_3Sc precipitates on the yield stress and work hardening of an Al–Mg–Sc alloy, *Acta Mater.*, 56(2008), No. 9, p. 1909.

[21] R.A. Karnesky, M.E. van Dalen, D.C. Dunand, and D.N. Seidman, Effects of substituting rare-earth elements for scandium in a precipitation-strengthened Al-0.08at.% Sc alloy, *Scripta Mater.*, 55(2006), No. 5, p. 437.

[22] Z.R. Nie, T.N. Jin, J.X. Zou, J.B. Fu, J.J. Yang, and T.Y. Zuo, Development on research of advanced rare-earth aluminum alloy, *Trans. Nonferrous Met. Soc. China*, 13(2003), No. 3, p. 509.

[23] Z.R. Nie, T.N. Jin, J.B. Fu, G.F. Xu, J.J. Yang, J.X. Zhou, and T.Y. Zuo, Research on rare earth in aluminum, *Mater. Sci. Forum*, 396-402(2002), p. 1731.

[24] S.P. Wen, Z.B. Xing, H. Huang, B.L. Li, W. Wang, and Z.R. Nie, The effect of erbium on the microstructure and mechanical properties of Al–Mg–Mn–Zr alloy, *Mater. Sci. Eng. A*, 516(2009), No. 1-2, p. 42.

[25] Z.G. Wu, M. Song, and Y.H. He, Effects of Er on the microstructure and mechanical properties of an as-extruded Al–Mg alloy, *Mater. Sci. Eng. A*, 504(2009), No. 1-2, p. 183.

[26] Z.M. Yin, J.F. Fang, J.W. Huang, B. Nie, C.Z. Shan, J.L. Guo, and L. Wang, Effects of aging treatment on intercrystalline corrosion and exfoliation corrosion behavior of 7A52 aluminum alloy, *J. Cent. South Univ. Sci. Technol.*, 38(2007), No. 4, p. 617.